Second virial coefficients of H_2 and its isotopologues from a six-dimensional potential

Giovanni Garberoglio,[1,a)] Piotr Jankowski,[2,b)] Krzysztof Szalewicz,[3,c)] and Allan H. Harvey[4,d)]

[1]*Interdisciplinary Laboratory for Computational Science (LISC), FBK-CMM and University of Trento, via Sommarive 18, I-38123 Povo (TN), Italy*
[2]*Department of Quantum Chemistry, Faculty of Chemistry, Nicolaus Copernicus University, Gagarina 7, PL-87-100 Toruń, Poland*
[3]*Department of Physics and Astronomy, University of Delaware, Newark, Delaware 19716, USA*
[4]*Thermophysical Properties Division, National Institute of Standards and Technology, 325 Broadway, Boulder, Colorado 80305, USA*

(Received 18 July 2012; accepted 21 September 2012; published online 17 October 2012)

We employ path-integral Monte Carlo techniques to compute the second virial coefficient as a function of temperature for molecular hydrogen (H_2), deuterium (D_2), and tritium (T_2), along with the mixed isotopologues HD, HT, and DT. The calculations utilize a new six-dimensional (6D) potential, which is derived by combining our previous high-quality ground-state 4D potential for the H_2 dimer with the 6D potential of Hinde. This new 6D potential is reduced to a set of 4D potentials by fixing the intramolecular coordinates at their expectation values for each temperature and isotopic combination. The results for H_2 are in good agreement with experimental data; the effect of the temperature dependence of the average bond length is only significant above approximately 1000 K. For D_2 and HD, the available experimental data are much more limited; our results agree with the data and provide reliable values at temperatures where no experimental data exist. For the species containing tritium, our results provide the only data available. © *2012 American Institute of Physics*. [http://dx.doi.org/10.1063/1.4757565]

I. INTRODUCTION

Hydrogen (H_2) is used in many industrial applications, and is often discussed as an energy carrier.[1] Knowledge of its thermodynamic properties is important in many of these applications; H_2 has been fairly well studied experimentally and a reference-quality equation of state (EOS) exists for vapor, liquid, and supercritical fluid conditions at temperatures up to 1000 K.[2]

Deuterium (D_2) and tritium (T_2) are of less practical importance, but they find some use in scientific investigations and in nuclear applications.[3] For D_2, a modest amount of data exists, but the only comprehensive fluid EOS we are aware of is unpublished and of limited accuracy.[4] Current efforts[5] to produce a state-of-the-art EOS for fluid D_2 provided part of the motivation for this work. For T_2, and also the heteronuclear isotopologues HD, HT, and DT, there are almost no experimental thermodynamic data, and no EOS has been proposed.

Thermodynamic properties in the gas phase can be described by the virial expansion, which gives a rigorous series of corrections to ideal-gas behavior

$$\frac{p}{\rho RT} = 1 + B(T)\rho + C(T)\rho^2 + \cdots. \quad (1)$$

In Eq. (1), p is the pressure, ρ the molar density, R the molar gas constant, and T the absolute temperature. The second virial coefficient $B(T)$ depends only on interactions between pairs of molecules, while the third virial coefficient $C(T)$ depends on interactions among three molecules. In this work, we focus on $B(T)$; Eq. (1) truncated after the first correction term is sufficient to provide accurate gas-phase thermodynamic properties at low and moderate pressures, and $B(T)$ can provide a useful boundary condition for fitting a more wide-ranging equation of state.

In 2008, together with other collaborators, we presented a high-accuracy 4D (rigid-rotor) potential-energy surface for the interaction of two H_2 molecules.[6] The bond length was fixed at the average distance for H_2 in its rovibrational ground state. We reported values of the second virial coefficient $B(T)$ computed from this potential with a path-integral Monte Carlo (PIMC) method. At temperatures above approximately 100 K, small systematic differences were observed from the best experimental data;[7] we speculated that this difference might be due to the neglect of rovibrational stretching of the H_2 molecule in our calculations. Because the length of the rigid rotor was fixed at the H_2 bond length, D_2 and other isotopologues (which have different bond lengths) were not addressed in the 2008 work.

In this work, we develop a new six-dimensional (6D) potential, described in Sec. II, based on our previous rigid-rotor potential[6] and on the 6D potential of Hinde.[8] This potential provides the best current description of H_2-H_2 interactions, which are relevant in many areas of physics, chemistry, and

a)garberoglio@fbk.eu.
b)teojan@chem.umk.pl.
c)szalewic@udel.edu.
d)Author to whom correspondence should be addressed. Electronic mail: allan.harvey@nist.gov.

engineering; two recent examples of scientific application of H_2-H_2 pair potentials are provided in Refs. 9 and 10.

We apply the new potential to address two issues. The first is the question of whether the rigid-monomer potential for H_2-H_2 (with the intramolecular H-H distance equal to its averaged ground-state value) is sufficient to describe $B(T)$, or whether the effect of rovibrational stretching at higher temperatures is significant. The second is the scarcity (and in some cases total absence) of accurate values of $B(T)$ for D_2 and other isotopologues.

II. INTERMOLECULAR POTENTIAL-ENERGY SURFACE

As discussed in Sec. III, our computations of $B(T)$ are performed at values of the intramolecular bond length that depend on temperature and on the isotopologue. This requires a full-dimensional interaction-energy surface $V(\boldsymbol{X}, r, s) = V(R, \theta_1, \theta_2, \phi, r, s)$, where $\boldsymbol{X} \equiv (R, \theta_1, \theta_2, \phi)$ defines the intermolecular geometry (R is the distance between the midpoints of the molecules, while θ_1, θ_2, and ϕ represent angular orientations; see Ref. 6) and r and s denote the intramolecular distances (which need not be identical, but will be in all our calculations here). The interaction energy V is defined as the difference between the total energy $E_{\rm tot}$ of the dimer and the sum of $E_{\rm tot}$ of the isolated monomers

$$V(\boldsymbol{X}, r, s) = E_{\rm tot}^{\rm H_2-H_2}(\boldsymbol{X}, r, s) - E_{\rm tot}^{\rm H_2}(r) - E_{\rm tot}^{\rm H_2}(s). \qquad (2)$$

Thus, the potential vanishes as $R \to \infty$ for any value of r and s.

We constructed a hybrid surface that combines the features of the surfaces published by Hinde[8] and by Patkowski *et al.*,[6] which will be denoted as $V_{\rm Hin}$ and $V_{\rm Pat}$, respectively. The $V_{\rm Hin}(\boldsymbol{X}, r, s)$ surface is six-dimensional, depending on all the inter- and intramolecular degrees of freedom, constructed on the basis of coupled clusters with single, double, and noniterative triple excitations [CCSD(T)] supermolecular calculations performed with the aug-cc-pVQZ+(3,3,2) mid-bond basis set,[11,12] supplemented with the complete triple excitations correction obtained with the aug-cc-pVTZ (without mid-bond) basis set.[11] The $V_{\rm Pat}(\boldsymbol{X})$ surface is four-dimensional, with the values of the H-H distances r and s set to the length of the bond averaged over the ground state of H_2, $r_0 = s_0 = 1.448736$ bohrs (1 bohr $\approx$ 0.052917721 nm). The interaction energies leading to $V_{\rm Pat}$ were obtained as a sum of three components: $E_{\rm int}^{\rm HF}$, $\delta E_{\rm int}^{\rm CCSD(T)}$, and $\delta E_{\rm int}^{\rm FCI}$. The Hartree-Fock component $E_{\rm int}^{\rm HF}$ was calculated in the aug-cc-pV5Z+(3,3,2,2,1) basis set.[6,11] The $\delta E_{\rm int}^{\rm CCSD(T)}$ energy was obtained from supermolecular CCSD(T) calculations with the aug-cc-pVQZ+(3,3,2,2,1) and aug-cc-pV5Z+(3,3,2,2,1) basis sets[6,11] followed by complete-basis-set extrapolation. The $\delta E_{\rm int}^{\rm FCI}$ component, which describes all post-CCSD(T) correlation corrections, was calculated using the full configuration interactions method in the aug-cc-pVDZ+(3,3,2) and aug-cc-pVTZ+(3,3,2) basis sets,[6,11] and also extrapolated. Thus, the level of theory employed to obtain the $V_{\rm Pat}$ surface was higher than in the case of $V_{\rm Hin}$. In Ref. 8, the computed *ab initio* interaction energy surface was empirically adjusted to better fit the experimental rovibrational transition energies of the dimer. However, $V_{\rm Hin}$ used in the present work is the original unadjusted surface.

To combine the higher accuracy of the $V_{\rm Pat}$ surface with the intramolecular flexibility of the $V_{\rm Hin}$ surface, we define the hybrid surface $V_{\rm HP}$ by the formula

$$V_{\rm HP}(\boldsymbol{X}, r, s) = V_{\rm Pat}(\boldsymbol{X}) + [V_{\rm Hin}(\boldsymbol{X}, r, s) - V_{\rm Hin}(\boldsymbol{X}, r_0, s_0)]. \qquad (3)$$

The surface defined by Eq. (3) is independent of the nuclear masses, so it may be used for any isotopologue; the masses only enter in determining the intramolecular distances r and s, as discussed in Sec. III A. By construction, $V_{\rm HP}$ becomes identical to $V_{\rm Pat}$ when $r = r_0$ and $s = s_0$. Since the reference separations are the averaged ground-state ones, $V_{\rm Pat}$ can be considered to correspond to the limit of zero temperature when only the ground state is occupied.

Functional forms of the $V_{\rm Pat}$ and $V_{\rm Hin}$ surfaces, described in Refs. 6 and 8, respectively, both represent the angular dependence with an expansion in coupled spherical harmonics. However, they differ substantially in details. The angular expansion coefficients of $V_{\rm Hin}$ depend not only on the intermolecular distance R, but also on two intramolecular distances r and s. The expansion coefficients of $V_{\rm Hin}$ for mid-range distances were calculated for 18 values of R and three values each of r and s. On the basis of these calculations, the potential routine generates the angular coefficients for any (R, r, s) using cubic splines for the R dependence and two-dimensional quadratic interpolation for the (r, s) dependence. For short-range distances, $R < 4.5$ bohrs, the interaction energy is obtained from a simple exponential formula that extrapolates expansion coefficients obtained for two grid points with shortest R. For large R, the expansion coefficients are calculated from van der Waals constants. The functional form of $V_{\rm Pat}$ is a sum of a short-range part and a damped long-range part. The long-range part is defined by the van der Waals constants, but more terms are taken into account than in the case of $V_{\rm Hin}$. The expansion coefficients of the short-range part explicitly depend on the intermolecular distance R, which makes the whole functional form R-dependent with no interpolation required. Moreover, the $V_{\rm Pat}$ short-range part has an exponential factor depending on R and on angular functions, which helps to properly represent the repulsive part of the surface. This exponential factor makes the $V_{\rm Pat}$ short-range term a nonlinear combination of angular functions, in contrast to the corresponding part of $V_{\rm Hin}$. The number of angular functions in $V_{\rm Pat}$ is significantly larger than in the case of $V_{\rm Hin}$. Although the angular terms used in the latter case are the largest components, the remaining neglected terms can make a noticeable contribution for some configurations of the dimer. However, the $V_{\rm HP}$ surface is only slightly biased by the limited angular representation of $V_{\rm Hin}$, since the $V_{\rm Pat}$ potential is the leading component of $V_{\rm HP}$.

In Fig. 1, we compare interaction energies obtained from different surfaces and calculated *ab initio* at the levels of accuracy of the $V_{\rm Hin}$ and $V_{\rm Pat}$ surfaces. The range of values of r corresponds to those used in our virial-coefficient calculations. There is a surprisingly large discrepancy between the values generated from $V_{\rm Hin}$ and the values calculated *ab initio*

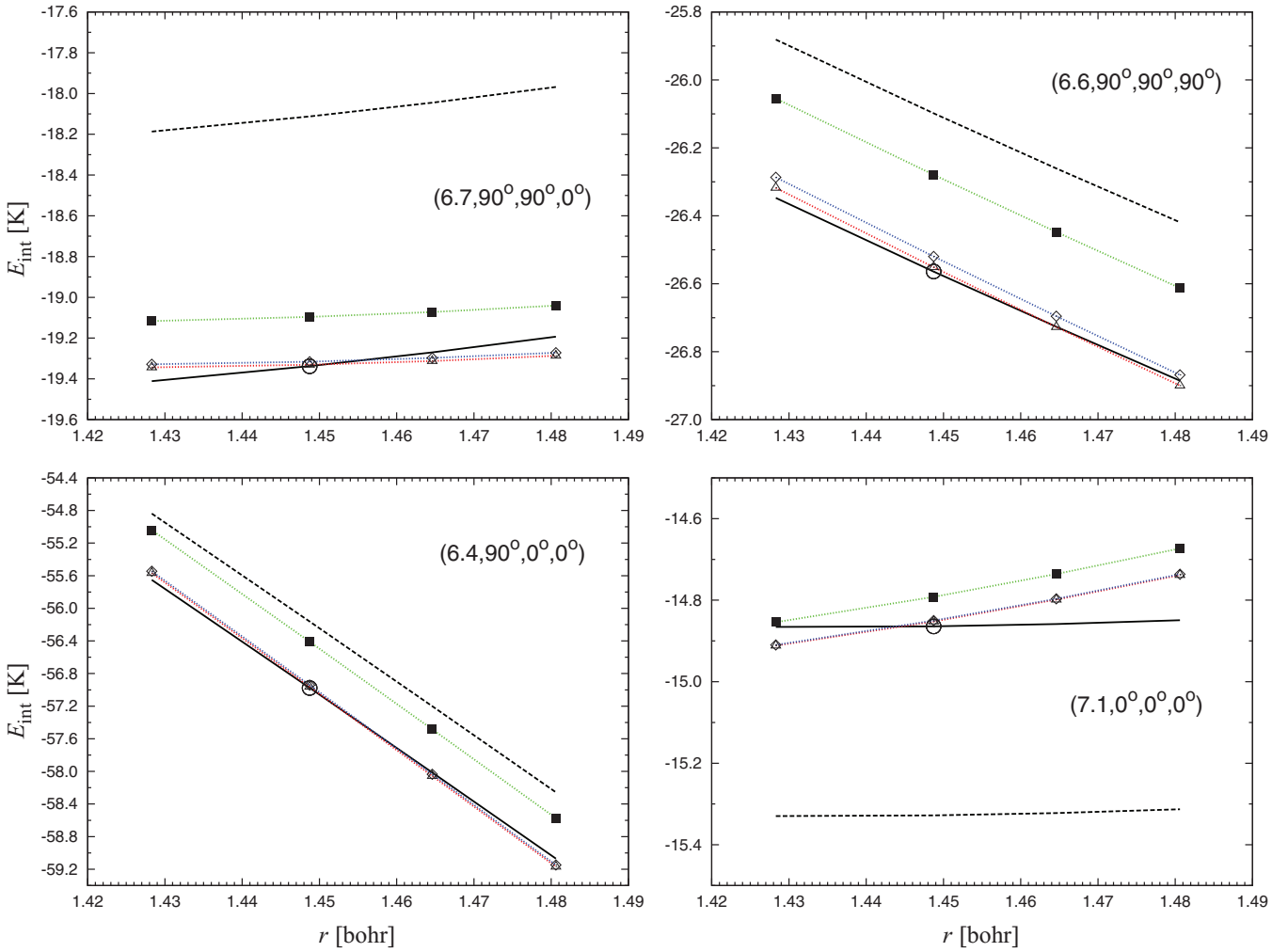

FIG. 1. Comparison of computed interaction energies E_{int} of H_2-H_2 for a few intermolecular orientations (R, θ_1, θ_2, ϕ) of the complex and for values of the H-H separation varying from 1.4283 to 1.4806 bohrs. The energies generated from V_{HP} are plotted with solid lines and the ones from V_{Hin} with dashed lines. Interaction energies calculated *ab initio* at the level of approximation of V_{Pat} are denoted by triangles, squares denote energies calculated at the same level as for the V_{Hin} surface, and diamonds denote energies computed in extended basis sets as described in the text. Dotted lines connecting these symbols are only guides to the eye. The circle in each panel indicates the energy and the H-H distance used in the construction of the V_{Pat} surface.

at the same level of approximation. Most likely this reflects inaccuracies of the fit in Ref. 8. On the other hand, this effect is almost quenched in the V_{HP} surface. This indicates that the inaccuracies in Ref. 8 are mainly in the intermolecular part, so that V_{Hin} correctly describes the effects of monomer deformations on interaction energies (the only feature of Ref. 8 we use). The comparison of the interaction energies given by V_{HP} and those calculated at the level of accuracy of V_{Pat} shows that the accuracy of V_{HP} can be regarded to be almost the same as that of V_{Pat}, at least for the tested range of r.

For the test geometries in Fig. 1, we also performed calculations for basis sets with cardinal numbers larger by one than those used in calculation of V_{Pat}. The components of the interaction energies have been obtained in the following basis sets: E_{int}^{HF} with aug-cc-pV6Z+(3,3,2,2,1),[6,13] $\delta E_{int}^{CCSD(T)}$ with aug-cc-pV5Z+(3,3,2,2,1) and aug-cc-pV6Z+(3,3,2,2,1) and extrapolation, and δE_{int}^{FCI} with aug-cc-pVTZ+(3,3,2) and aug-cc-pVQZ+(3,3,2) and extrapolation. The largest discrepancy between interaction energies obtained with these basis sets and their V_{Pat} counterparts is 0.03 K, which confirms that the good performance of the basis sets used to calculate V_{Pat} in Ref. 6 is still valid for slightly distorted geometries of H_2.

For 16 geometries of the complex shown in Fig. 1, corresponding to four intermolecular orientations and four intramolecular distances, the largest discrepancy of the V_{HP} energies from the values calculated at the level of accuracy of the V_{Pat} surface is 0.11 K and the root-mean-square value of these discrepancies is 0.07 K. In particular, for the (6.4,90,0,0) geometry, close to the minimum of the interaction-energy surface, the discrepancy is 0.1 K, which is close to 0.2% of the energy at the minimum. Thus, since in Ref. 6 the uncertainty of V_{Pat} close to the energy minimum was estimated to be 0.15 K or 0.3% (which is probably overly conservative in light of the 0.03 K difference obtained with extended basis sets as described above), we can conservatively estimate the uncertainty of the minimum of the V_{HP} surface to be 0.25 K or 0.5%. Moreover, in Ref. 6 the error of all energies in the negative-energy region was estimated to be at most 0.5 K, and this value can be modified by the additional uncertainty 0.1 K,

arising from the H_2 flexibility described by the V_{Hin} surface, to be equal to 0.6 K for V_{HP}. Thus, we can extend conclusions regarding the accuracy of the V_{Pat} surface given in Ref. 6 to the V_{HP} surface, with only small modifications.

In order to make uncertainty estimates for $B(T)$, we constructed upper and lower perturbed potentials based on these estimates of the accuracy of V_{HP} as follows: (a) for energies above 1000 K, shift by 0.3%; (b) for energies between 100 K and 1000 K, shift by 0.7%; (c) for positive energies near the repulsive core less than 100 K, shift by 1 K; (d) for energies less than −50 K, shift by 0.25 K; (e) for negative energies with magnitudes less than 50 K, shift by 0.6 K at distances less than the minimum of the potential well, and by $\min(0.25\text{ K}, |0.003 V_{HP}|)$ at larger distances; (f) for positive energies at large distances (possible at some configurations due to the quadrupole-quadrupole interaction), shift by 0.3%. While these uncertainty estimates are non-statistical, experience has shown that earlier estimates of this type are in most cases confirmed by later, more accurate calculations. For purposes of comparing with experiment and estimating the uncertainty in $B(T)$, we believe it is reasonable to associate these shifted potentials with an uncertainty corresponding to a 95% confidence interval.

The supplementary material[14] includes documentation and computer code for the V_{HP} potential. The computer code is a straightforward combination, according to Eq. (3), of the code provided in the online supplementary materials of Refs. 6 and 8; in the case of Ref. 8, the newer version of the supplement created in 2010 has been used. The V_{HP} surface has been used in the present project for a very limited range of r and s. While V_{HP} can also be applied for other H-H separations, one should remember that, due to the way it was constructed, V_{Hin} is most reliable for values of r and s between 1.1 and 1.7 bohrs; this limitation is inherited by V_{HP}. Using V_{HP} for more stretched monomers can produce unphysical results, especially for small values of R.

III. CALCULATION METHODS

A. Equilibrium bond length

In principle, calculation of $B(T)$ from V_{HP} could involve a matrix of interactions between pairs of molecules at different bond lengths, covering the entire thermally weighted distribution of rovibrational states. This is impractical with present resources, as is a PIMC calculation of $B(T)$ for the full flexible 6D potential, for which no practical algorithm has been developed to our knowledge. However, a reasonable approximation for the effect of stretching with temperature is obtained by computing the expectation value of the bond length $\langle r\rangle_T$ at each temperature T, and computing $B(T)$ between two of these "average" molecules with bond length $\langle r\rangle_T$ applying the interaction potential $V_T(\boldsymbol{X}; T) = V_{HP}(\boldsymbol{X}, \langle r\rangle_T, \langle r\rangle_T)$.

The average bond length of the molecule can be formally defined as

$$\langle r\rangle_T = \sum_{n,J} p(n, J; T)\, \langle \chi_{nJ} | r | \chi_{nJ}\rangle, \tag{4}$$

where the quantum numbers n and J define the vibrational and rotational state of H_2, respectively, while χ_{nJ} denotes the corresponding wave function. The fractional population of the (n,J) state is given by the formula

$$p(n, J; T) = \frac{(2J+1)\exp(-E(n, J)/T)}{\sum_{n', J'}(2J'+1)\exp(-E(n', J')/T)}, \tag{5}$$

where $E(n',J')$ is the energy of the (n',J') state.

The matrix elements $\langle \chi_{nJ}|r|\chi_{nJ}\rangle$ needed for evaluation of $\langle r\rangle_T$ for the H_2 isotopologues were calculated using the H-H component of the H_3 potential developed by Mielke *et al.*[15] (assuming a singlet configuration for the electronic spin). This H-H component was a fit performed by the authors of Ref. 15 to accurate calculations for H_2 by Kolos *et al.*[16] Use of a separate H-H potential for this purpose is necessary because the V_{HP} potential used in the rest of our work is strictly intermolecular in nature and does not contain the H-H intramonomer potential.

The radial Schrödinger equation describing the nuclear motion in H_2 was solved as a function of the angular momentum of the molecule in the basis spanned by the eigenfunctions of a particle confined in a one-dimensional box. We found that a box extending from 0.02 nm to 0.2 nm in the radial coordinate was large enough to provide well-converged results in the whole range of temperature investigated. The program also takes into account the possibility of restricting the rotational states to either even or odd angular momenta.

As is well known, the angular momentum of homonuclear diatomic molecules is limited by quantum statistics to even or odd multiples of $\hbar$ (Planck's constant divided by 2π), depending on the nuclear-spin state. In the case of H_2 and T_2, the molecules for which only even rotational states are allowed are called *para*, and those having only odd rotational states are called *ortho*. The reverse nomenclature applies to D_2. No such restriction exists for heteronuclear molecules, whose angular momentum can take any value.

All the allowed rovibrational eigenfunctions with energy $E/k_B < 5 \times 10^4$ K (where k_B is the Boltzmann constant and the zero of E is set at the bottom of the potential well) were used to calculate the thermal averages giving the molecular bond length. This energy cutoff is within 4% of the dissociation limit and was completely sufficient to converge the calculations at the temperatures considered. The actual number of states used in Eqs. (4) and (5) depended on the isotopologue, with typical values ranging from ∼100 in the case of *para*-H_2 to ∼500 in the case of DT.

The resulting expectation values of the bond length are shown in Fig. 2 as a function of temperature for H_2, D_2, T_2, and HD (HT and DT are omitted for clarity). The bond length is larger for the smaller-mass isotopologues and increases with temperature. The relative variation of bond length at $T = 2000$ K with respect to the zero-temperature (i.e., ground-state) value ranges between 2% and 2.7% in the cases of H_2 and T_2, respectively.

B. Second virial coefficient

The second virial coefficient $B(T)$ was calculated as described in Ref. 6, with only minor differences in procedures as described below.

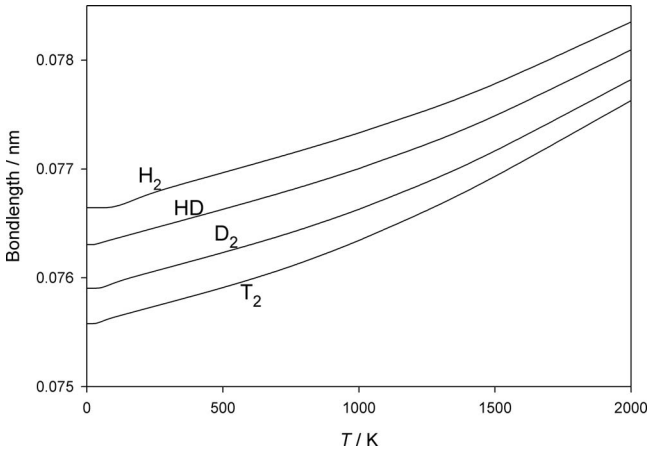

FIG. 2. Expectation value of intramolecular bond length for isotopologues of molecular hydrogen as a function of temperature.

The semiclassical values in the present work, used only for estimating the effect of molecular stretching on $B(T)$, have been obtained by performing nested integrations with the adaptive Gauss-Kronrod method with a relative tolerance of 10^{-3}.

In the PIMC algorithm, the VEGAS method[17] was used to perform the radial integration. This procedure turned out to be more efficient than that described in Ref. 6, while producing results of comparable quality. The statistical uncertainty of the PIMC algorithm was evaluated by averaging the results of two sets of 16 independent calculations. In the first set of calculations, the rotational degrees of freedom were evaluated with the hybrid Monte Carlo method described in Ref. 18, whereas in the second set we sampled the rotational degrees of freedom with the algorithm described in Ref. 19. These two sets gave consistent results (within statistical uncertainty), thus validating the efficiency of rotational sampling.

The value of the Trotter index P (which characterizes the degree of discretization of the path integral; see Ref. 6) was chosen according to $P = \alpha_I/T + 7$, where α_I depends on the isotopologue I. The values of α_I are reported in Table I. We confirmed that this way of assigning P resulted in good convergence of the path-integral results at all the temperatures studied.

The path-integral method can straightforwardly be used to perform calculations on molecules with even angular momentum states (that is, *para*-H_2, *ortho*-D_2, and *para*-T_2), but the rotational density matrix is not positive definite for homonuclear diatomics having only odd angular momentum states, resulting in more demanding calculations.[20,21] In order to quantify the importance of the *ortho* or *para* nature of homonuclear hydrogen isotopologues in the determination of $B(T)$, we compared the results obtained using only even angular momentum states to the values of $B(T)$ calculated assuming (unphysical) homonuclear molecules having access to all rotational states. We found that the values of the second virial coefficient obtained in the two cases were the same within the statistical uncertainty of our calculations, which in turn is much smaller than the uncertainty of $B(T)$ due to the accuracy of the pair potential. For these reasons, we do not distinguish between the rotational states of the homonuclear isotopologues in the following discussion, and all of our results are reported for the simplified case where spin statistics are ignored.

TABLE I. Values of the parameter α_I used to calculate the Trotter index P in the PIMC calculations of $B(T)$.

Isotopologue I	α_I (K)
H_2	2500
D_2	1800
T_2	1200
HD	1800
HT	1800
DT	1500

IV. CALCULATIONS FOR H_2

A. Results and comparison with experiment

Table II shows values of $B(T)$ for H_2 at temperatures from 15 K to 2000 K, calculated as described in Sec. III with the

TABLE II. Computed second virial coefficient $B(T)$ for H_2 along with its expanded uncertainty $U(B)$, and $\Delta B_{\text{stretch}}$ which is the contribution to B from molecular stretching beyond the ground-state length.

T (K)	B (cm^3 mol^{-1})	$U(B)$ (cm^3 mol^{-1})	$\Delta B_{\text{stretch}}$ (cm^3 mol^{-1})
15	− 222.16	2.59	
20	− 146.93	1.85	
25	− 106.17	1.31	
30	− 80.55	1.05	
35	− 63.06	0.85	
40	− 50.44	0.72	
45	− 40.88	0.63	
50	− 33.32	0.56	
60	− 22.50	0.49	
75	− 12.03	0.37	
90	− 5.37	0.32	
100	− 2.18	0.26	− 0.006
125	3.42	0.22	− 0.011
150	6.93	0.21	− 0.015
175	9.33	0.17	− 0.018
200	10.99	0.16	− 0.019
225	12.24	0.14	− 0.019
250	13.16	0.13	− 0.018
273.16	13.84	0.13	− 0.016
300	14.43	0.11	− 0.015
350	15.21	0.11	− 0.011
400	15.69	0.09	− 0.007
450	16.00	0.09	− 0.004
500	16.19	0.09	0.000
550	16.29	0.08	0.003
600	16.36	0.07	0.007
700	16.35	0.06	0.014
800	16.26	0.06	0.020
900	16.12	0.06	0.027
1000	15.96	0.05	0.034
1200	15.60	0.04	0.047
1500	15.05	0.04	0.068
2000	14.22	0.03	0.106

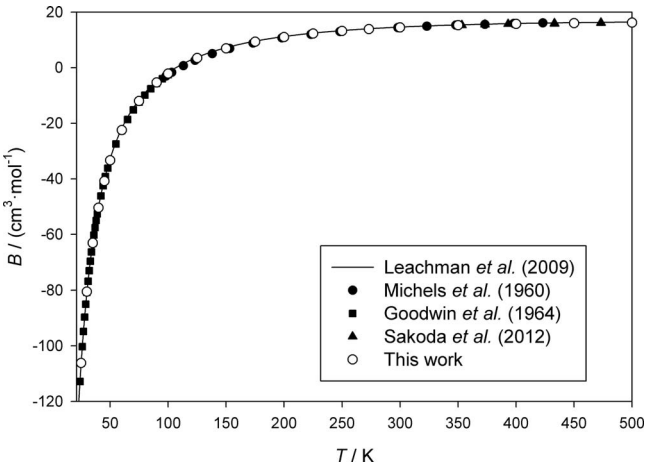

FIG. 3. Experimental data and calculated values for the second virial coefficient $B(T)$ for H_2.

potential described in Sec. II. These results supersede the PIMC values given in our previous work,[6] which neglected the temperature dependence of the bond length (although, as we shall see below, this has a very small influence on $B(T)$ below 600 K, which was the upper temperature limit of calculations in Ref. 6).

There have been many experimental studies of $B(T)$ for H_2; these are summarized by Leachman *et al.*[2] We restrict our comparisons to two of the most comprehensive and accurate sources at temperatures above[7] and below[22] 100 K, along with some recently published data[23] that extend to somewhat higher temperatures.

Figure 3 shows these experimental data, along with our results and $B(T)$ calculated from the EOS of Leachman *et al.*[2] as implemented in NISTs REFPROP (Ref. 24) database. Uncertainties are not shown because they would be difficult to see on the scale of Fig. 3. While Fig. 3 demonstrates the general consistency of the results, a different approach to displaying the data is required in order to make a detailed comparison.

In Figs. 4 and 5, we have plotted the difference between the various experimental data and B calculated from the EOS of Leachman *et al.*[2,24] at the temperature of the experiment. Our results are shown relative to the same reference. Figure 4 covers temperatures up to 100 K; higher temperatures are shown in Fig. 5. Because Goodwin *et al.*[22] reported smoothed data at closely spaced temperatures, some of their points are omitted for clarity in Fig. 4. The experimental error bars represent expanded uncertainties with coverage factor $k = 2$ (approximately a 95% confidence interval); for our results the expanded uncertainties are estimated as described in Sec. IV B. No error bars are shown for the data of Sakoda *et al.*[23] in Fig. 5, because no uncertainties in B were reported in Ref. 23.

Below 100 K, Fig. 4 shows that our results are consistent with the experimental data within mutual uncertainties; our uncertainties are somewhat smaller than those of Goodwin *et al.*[22] at the high end of this temperature range, and somewhat larger at the low end. In Fig. 5, we see excellent agreement with the high-temperature data of Sakoda *et al.*[23]

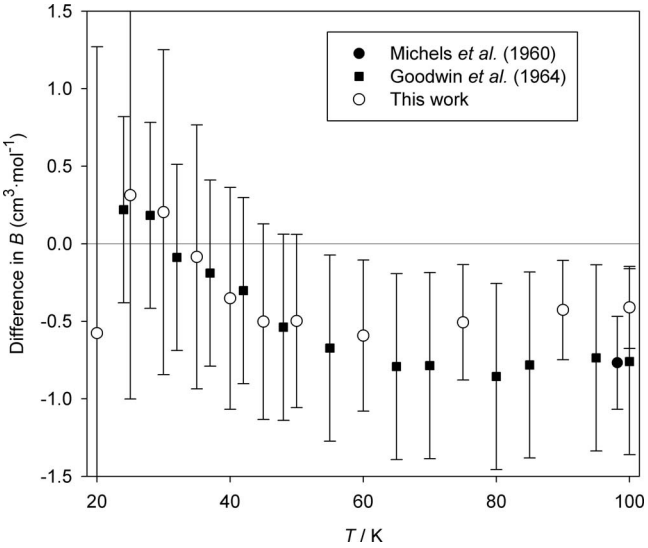

FIG. 4. Differences at low temperatures between experimental and PIMC values of $B(T)$ for H_2 and values of $B(T)$ calculated from the EOS of Leachman *et al.*[2]

Agreement with the data of Michels *et al.*[7] is generally within mutual uncertainties, but there seems to be a slightly different temperature trend, and there is a region around 125 K where the error bars just barely overlap. The EOS of Leachman *et al.*,[2] which was not fitted to any virial data, systematically overpredicts $B(T)$ at temperatures above about 40 K, but only by a small amount, less than 0.5 cm^3 mol^{-1}.

B. Uncertainty analysis

The uncertainty estimates $U(B)$ given in Table II were obtained by combining the contributions from the uncertainty of the pair potential and from the convergence of the PIMC calculations, in a manner similar to previous work on helium.[25]

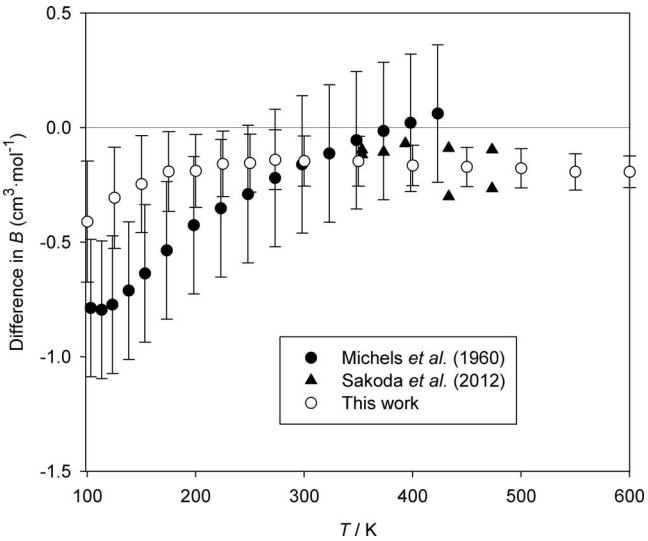

FIG. 5. Differences at high temperatures between experimental and PIMC values of $B(T)$ for H_2 and values of $B(T)$ calculated from the EOS of Leachman *et al.*[2]

The contribution due to PIMC convergence was estimated as the standard deviation σ_{PIMC} of the mean from 32 independent Monte Carlo runs. For the contribution from uncertainty in the potential, we constructed perturbed potentials that were shifted to higher energies and to lower energies as described in Sec. II. The corresponding uncertainty in B is therefore one-half of the difference between $B(T)$ calculated with the upper and lower perturbed potentials. PIMC calculations were carried out on the perturbed potentials to evaluate this difference. This gave an accurate representation of the difference despite the uncertainty in PIMC convergence, because the PIMC uncertainty at these conditions is approximately an order of magnitude smaller than the uncertainty contribution due to the potential. The expanded uncertainty $U(B)$ (coverage factor $k = 2$, approximately corresponding to a 95% confidence interval) is then obtained by combining (in quadrature) this contribution from the uncertainty of the potential with the contribution $2\sigma_{\mathrm{PIMC}}$ from the PIMC convergence.

These uncertainties do not include additional uncertainty resulting from our neglect of monomer-flexibility effects. This source of error will be discussed further in Sec. VII.

C. Effect of molecular stretching with temperature

Table II also includes, for temperatures of 100 K and above, the quantity $\Delta B_{\mathrm{stretch}}$, which is the difference between B computed with the new potential V_{HP} at the average "stretched" value $\langle r \rangle_T$ and that computed from the $r = r_0$ potential V_{Pat}. Because this difference is small, of similar magnitude to the uncertainty due to PIMC convergence, we computed it with semiclassical calculations as described in Sec. III B, which can be converged much more tightly. This is a reasonable approximation, since molecular stretching is negligible at the low temperatures where the semiclassical approximation loses accuracy.

It can be seen that $\Delta B_{\mathrm{stretch}}$ is relatively small up to quite high temperatures, only reaching 0.1 $\mathrm{cm^3\ mol^{-1}}$ as the temperature nears 2000 K. Interestingly, it is negative at temperatures between about 100 K and 500 K, becoming positive at higher temperatures; we will discuss this behavior in Sec. VII. $\Delta B_{\mathrm{stretch}}$ only becomes significant (in the sense of having a magnitude comparable to the expanded uncertainty) at temperatures above approximately 1000 K.

V. CALCULATIONS FOR D_2

Table III shows $B(T)$ and its expanded uncertainty $U(B)$ for D_2. The calculations, including uncertainty calculations, were performed in the same manner as for H_2.

Experimental $B(T)$ data for D_2 are relatively sparse. Michels *et al.* reported virial coefficients for D_2 between roughly 98 K and 423 K in the same paper as their H_2 results.[7] Schäfer[26] reported $B(T)$ from volumetric measurements at subatmospheric pressures between approximately 23 K and 46 K. Beenakker *et al.*[27] reported one value of B at 20.4 K. Varekamp and Beenakker[28] made differential measurements that extended the results of Ref. 27 down to 18 K, while Knaap *et al.*[29] similarly extended the results up to 70 K.

TABLE III. Computed second virial coefficient $B(T)$ for D_2 along with its expanded uncertainty $U(B)$, and $\Delta B_{\mathrm{stretch}}$ which is the contribution to B from molecular stretching beyond the ground-state length.

T (K)	B ($\mathrm{cm^3\ mol^{-1}}$)	$U(B)$ ($\mathrm{cm^3\ mol^{-1}}$)	$\Delta B_{\mathrm{stretch}}$ ($\mathrm{cm^3\ mol^{-1}}$)
15	−283.78	3.76	
20	−179.17	2.11	
25	−126.16	1.61	
30	−94.35	1.20	
35	−73.21	0.92	
40	−58.34	0.79	
45	−47.31	0.67	
50	−38.67	0.63	−0.007
60	−26.34	0.48	−0.012
75	−14.70	0.43	−0.020
90	−7.31	0.32	−0.025
100	−3.80	0.27	−0.027
125	2.27	0.24	−0.029
150	6.05	0.21	−0.028
175	8.60	0.18	−0.026
200	10.42	0.15	−0.024
225	11.74	0.13	−0.022
250	12.72	0.13	−0.020
273.16	13.44	0.12	−0.018
300	14.08	0.11	−0.015
350	14.92	0.19	−0.011
400	15.44	0.09	−0.007
450	15.78	0.08	−0.004
500	16.00	0.08	0.000
550	16.12	0.08	0.004
600	16.19	0.07	0.007
700	16.21	0.06	0.015
800	16.13	0.06	0.022
900	16.00	0.05	0.029
1000	15.84	0.05	0.036
1200	15.50	0.04	0.051
1500	14.97	0.04	0.076
2000	14.16	0.03	0.121

Therefore, the $B(T)$ data of Refs. 27–29 are not independent; they are all tied to the 20.4 K datum of Beenakker *et al.*[27]

Figure 6 compares our results (Table III) with the literature data at temperatures below 75 K. A similar comparison is shown in Fig. 7 for the data of Michels *et al.*[7] In both cases, the agreement is excellent. Uncertainties for the PIMC results on Figs. 6 and 7 would be smaller than the size of the symbols.

Table III also shows $\Delta B_{\mathrm{stretch}}$ for D_2. The effect of stretching on $B(T)$ is very similar to that shown in Table II for H_2; a small difference is seen at low temperatures where rotational levels above the ground state become significantly occupied at a lower temperature for D_2 than for H_2 (this is also seen in the behavior at the lowest temperatures of the average bond length in Fig. 2).

VI. CALCULATIONS FOR T_2, HD, HT, AND DT

In Table IV, we give $B(T)$ for the other four isotopologues of molecular hydrogen. No uncertainty analysis was performed for these species, but the uncertainties should be

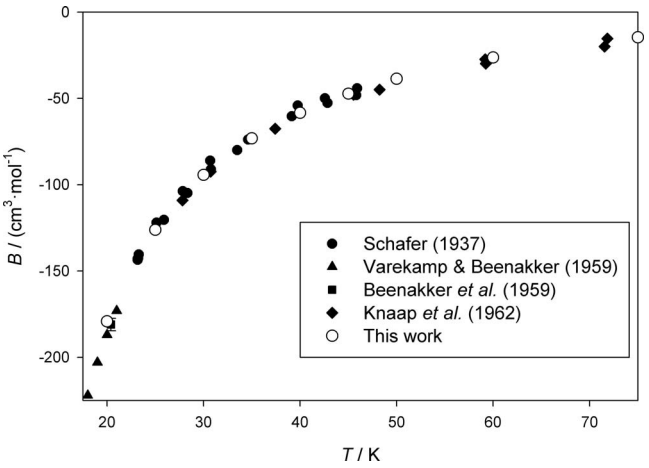

FIG. 6. Low-temperature data for $B(T)$ of D_2.

similar to those shown in Tables II and III for H_2 and D_2, as should the values of $\Delta B_{\text{stretch}}$.

The only one of these isotopologues with experimental data is HD, for which $B(T)$ values were obtained by the group of Beenakker.[27–29] As with D_2, this consisted of a single datum at 20.4 K,[27] which was extended to other temperatures by differential measurements.[28,29] Figure 8 shows these data along with our results; the agreement is good.

VII. DISCUSSION

We used path-integral methods to derive values of $B(T)$ for H_2 and its isotopologues over a wide range of temperatures. For H_2, our results generally confirm existing experimental data and extend the temperature range. For D_2 and HD, our results are in agreement with the limited data available, and provide values at many conditions where no data exist. For T_2, HT, and DT, no experimental data exist, so that our work provides data where none existed before.

At all conditions examined here, the uncertainty in $B(T)$ is dominated by the uncertainty in the pair potential; the contribution from imperfect convergence of the PIMC calculation is roughly an order of magnitude smaller. This means that a fruitful path for reducing the uncertainty in $B(T)$ for these species would be further refinement of the pair potential.

There is additional uncertainty due to our use of a single expectation value of the bond length, calculated according

TABLE IV. Computed second virial coefficient $B(T)$ for HD, HT, DT, and T_2.

	B (cm^3 mol^{-1})			
T (K)	HD	HT	DT	T_2
15	− 260.28	− 285.36	− 300.88	− 314.41
20	− 167.56	− 180.17	− 187.72	− 194.03
25	− 119.25	− 126.93	− 131.14	− 134.93
30	− 89.52	− 94.99	− 97.80	− 100.08
35	− 69.83	− 73.73	− 75.73	− 77.45
40	− 55.65	− 58.72	− 60.25	− 61.44
45	− 45.16	− 47.60	− 48.75	− 49.76
50	− 36.95	− 38.99	− 39.88	− 40.67
60	− 25.10	− 26.55	− 27.21	− 27.77
75	− 13.86	− 14.86	− 15.32	− 15.67
90	− 6.75	− 7.47	− 7.80	− 8.05
100	− 3.30	− 3.92	− 4.18	− 4.40
125	2.59	2.16	2.00	1.86
150	6.30	6.00	5.88	5.77
175	8.82	8.55	8.47	8.38
200	10.59	10.38	10.31	10.24
225	11.87	11.72	11.64	11.57
250	12.86	12.70	12.65	12.58
273.16	13.56	13.42	13.36	13.30
300	14.19	14.06	14.01	13.97
350	15.01	14.90	14.85	14.82
400	15.52	15.43	15.40	15.36
450	15.85	15.78	15.74	15.70
500	16.06	16.00	15.95	15.93
550	16.17	16.13	16.09	16.06
600	16.25	16.19	16.16	16.13
700	16.27	16.22	16.18	16.16
800	16.17	16.13	16.10	16.08
900	16.04	16.01	15.97	15.95
1000	15.89	15.86	15.82	15.80
1200	15.54	15.51	15.48	15.46
1500	15.00	14.98	14.95	14.94
2000	14.19	14.17	14.15	14.14

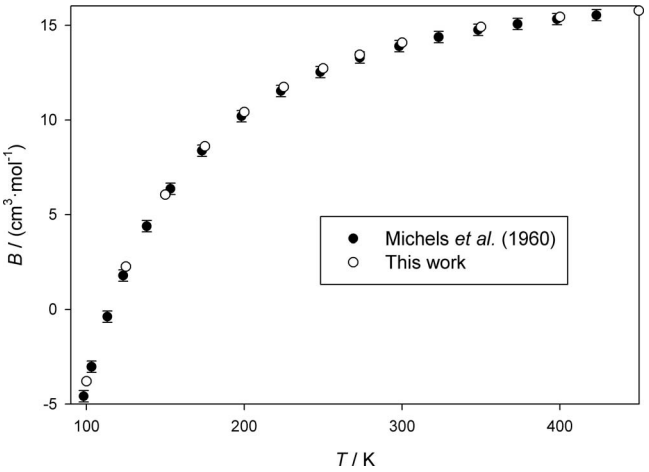

FIG. 7. Comparison of calculated values of $B(T)$ for D_2 to those reported by Michels *et al.*[7]

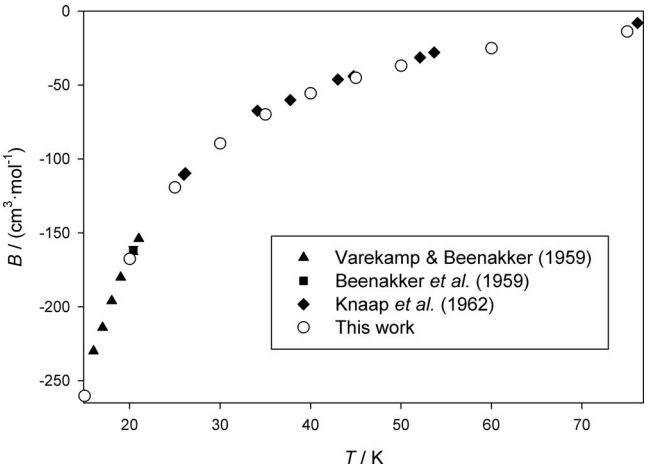

FIG. 8. Low-temperature data for $B(T)$ of HD.

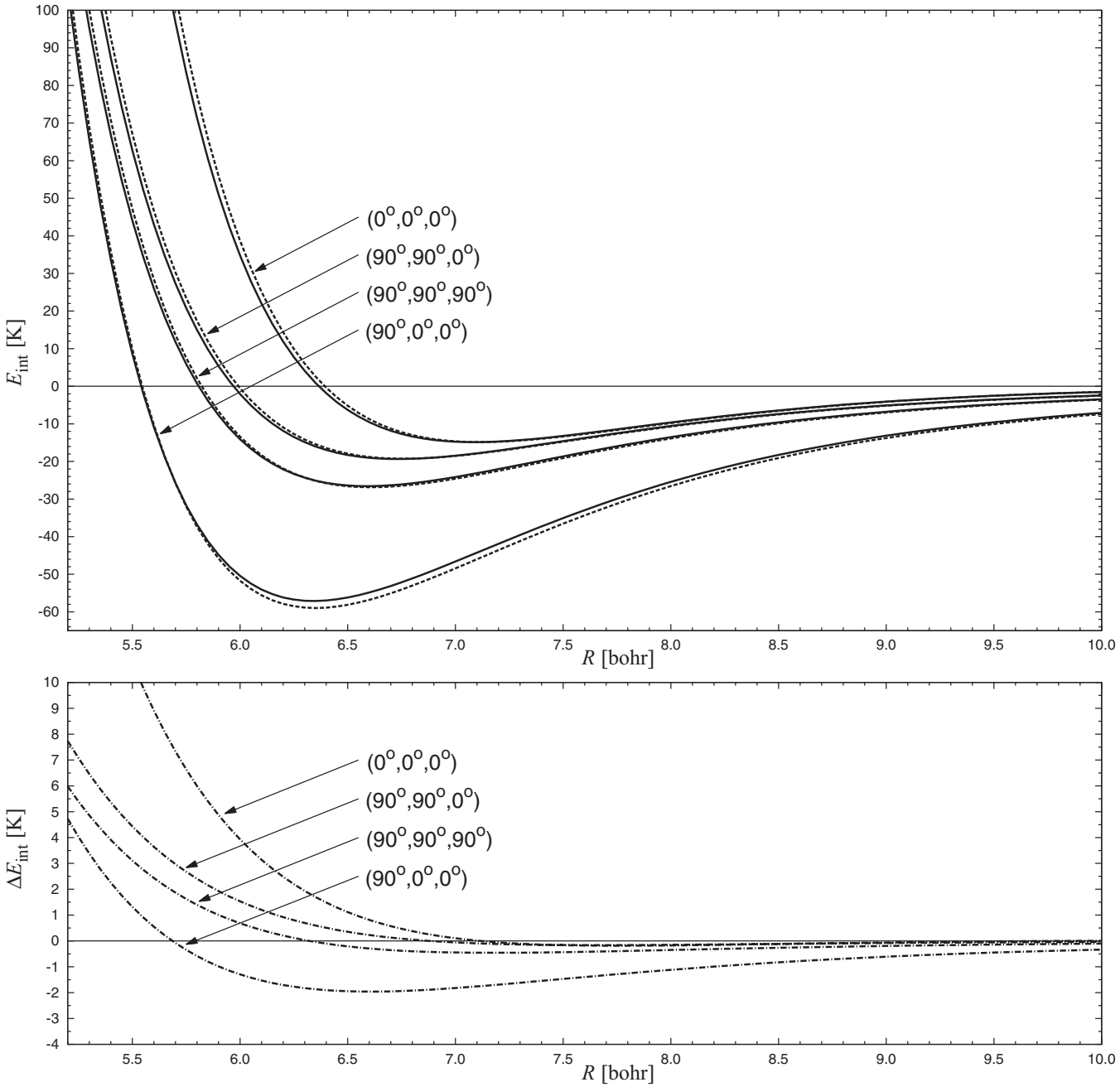

FIG. 9. Change of pair potential energy with stretching as a function of radial distance R for four different angular orientations. In the top panel, the solid curve is the potential with the bond length for each H_2 molecule at its ground-state value r_0, while the dashed line shows the potential when each molecule has bond length $1.02r_0$. The bottom panel shows the difference between the stretched and r_0 potential.

to Eq. (4), to represent the molecules. Such a calculation neglects the effect of monomer flexibility on interaction energies. A more rigorous interaction energy can be obtained by calculating the distribution of rovibrational states at each temperature, and for each combination of states averaging the interaction energy over the vibration (rather than computing the energy at a single vibrationally-averaged geometry). This can be expressed as

$$\langle V\rangle_T(\boldsymbol{X};T) = \sum_{n,J}\sum_{n',J'} p(n,J;T)p(n',J';T) \times \langle \chi_{nJ}\chi_{n'J'}|V_{\rm HP}(\boldsymbol{X},r,s)|\chi_{nJ}\chi_{n'J'}\rangle. \quad (6)$$

The matrix element in Eq. (6) can be computed as a two-dimensional integration over the bond lengths r and s, where χ_{nJ} and $\chi_{n'J'}$ are functions of r and s, respectively. It has been shown in Ref. 30 that the use of intermolecular potentials averaged over monomer vibrations results in spectra of van der Waals complexes that are much closer to full-dimensional spectra than any rigid-monomer results.

While the computational requirements of using Eq. (6) within a complete PIMC calculation of $B(T)$ were prohibitive, we can estimate the error in interaction energy introduced by our use of an average bond length by evaluating Eq. (6) at selected configurations. For this purpose, we obtained the wave functions χ_{nJ} for H_2 with the method of Cooley[31] and the

potential of Ref. 16. While the summations in Eq. (6) are infinite in principle, in practice only a limited number of rovibrational states contribute significantly; even at 2000 K only 23 states have $p(n, J; T)$ larger than 0.0001. We evaluated Eq. (6) at eight configurations (four with negative interaction energies; four with positive energies) at 0 K, 100 K, 1000 K, and 2000 K. In all cases, $\langle V \rangle_T$ from Eq. (6) was higher (more positive or less negative) than V_T obtained by our average bond length method described in Sec. III A; the relative differences were typically in the range 0.5%–1%, of similar magnitude to the uncertainty in the V_{HP} surface itself. The differences were slightly larger at high temperatures, but the bulk of the difference is present even at 0 K, consistent with previous results[30] showing that, even in the ground state, error of this magnitude is introduced if one computes a property at an averaged bond length rather than averaging the property over the vibration.

Therefore, there is a small but not negligible systematic error in our interaction energies used in the calculations of $B(T)$. The direction of the error is such that the values for H_2 in Table II are likely systematically too low by an amount perhaps as large as the uncertainty contribution due to the uncertainty of the potential, which is the majority of $U(B)$. We note that this error will be proportionally smaller for the higher-mass isotopologues reported in Tables III and IV, because of the smaller amplitudes of their vibrations.

In principle, these effects could also be accounted for in a fully six-dimensional PIMC calculation of $B(T)$. This would also require a large increase in computational resources, in addition to being complicated by the deficiencies in the potential at long bond lengths mentioned at the end of Sec. II. Both the 6D calculation of $B(T)$ and calculation using $\langle V \rangle_T$ from Eq. (6) will be the subject of future work.

As seen in Tables II and III, stretching of the molecule due to higher rovibrational states does not contribute significantly to $B(T)$ except above approximately 1000 K. This means that, contrary to the speculation in Ref. 6, such stretching does not account for the small systematic difference between our results for H_2 and the experimental data of Michels *et al.*[7] We note that, while we cannot yet precisely quantify the monomer-flexibility effect on $B(T)$ mentioned above, that effect would be of the wrong sign to account for this difference.

The change of sign of $\Delta B_{\text{stretch}}$ is an interesting phenomenon. Physically, it is reasonable that the negative $\Delta B_{\text{stretch}}$ at low temperatures arises from dispersion forces due to the increased polarizability of the stretched molecule; such an increase in polarizability for H_2 has been predicted by *ab initio* calculations[32] and observed in precise measurements of the dielectric permittivity.[33] Figure 9, in which V_{HP} is plotted for four orientations as a function of R both in the ground state and when stretched by a factor of 1.02, shows that the attractive part of the stretched potential lies below the potential with bond length r_0. At high temperatures, dispersion forces become unimportant and $B(T)$ is dominated by repulsive forces, so $\Delta B_{\text{stretch}}$ would become positive due to the increased excluded volume of the stretched molecules which is also evident in Fig. 9.

With straightforward modifications, the method applied here could be used to calculate values of "cross" second virial coefficients characterizing the interactions of two unlike molecules. Such values would be useful in modeling the thermodynamics of mixtures of isotopologues, as might be encountered in separations for proposed fusion systems.[3]

In order to describe thermodynamics at higher densities, the third virial coefficient $C(T)$ is useful. Some experimental $C(T)$ values have been published for H_2 (Refs. 7 and 22) and D_2 (Ref. 7), but their uncertainties are relatively large. With significantly more computational expense, path-integral methods could be applied to $C(T)$, as has been done for helium.[25] To do this quantitatively requires a description of the three-body nonadditive potential; the commonly used Axilrod-Teller potential, which accounts only for dispersion interactions, has been shown[34] to be inadequate for three H_2 molecules at distances that would characterize collisions at temperatures of practical interest. To our knowledge, the only complete three-body surface for H_2 was recently developed by Manzhos *et al.*;[35] this could be applied in concert with PIMC methods to compute $C(T)$ for H_2, and since the three-body contribution is not large it should be reasonable to use a three-body potential with r fixed at its H_2 value in calculations for other isotopologues as well.

ACKNOWLEDGMENTS

We thank I.A. Richardson for information about sources of experimental data for D_2 and HD, J.W. Leachman for helpful discussions on data needs for H_2 isotopologues, and R.J. Hinde for a useful discussion of 6D potentials. We thank an anonymous referee for suggesting the calculation using Eq. (6). The path-integral calculations were performed on the KORE computer cluster at Fondazione Bruno Kessler. K.S. was supported by National Science Foundation (NSF) Grant No. CHE-1152899.

[1]The Department of Energy Hydrogen and Fuel Cells Program Plan (U.S. Department of Energy, Washington, DC, 2011).
[2]J. W. Leachman, R. T Jacobsen, S. G. Penoncello, and E. W. Lemmon, J. Phys. Chem. Ref. Data **38**, 721 (2009).
[3]M. Glugla, A. Antipenkov, S. Beloglazov, C. Caldwell-Nichols, I. R. Cristescu, I. Cristescu, C. Day, L. Doerr, J.-P. Girard, and E. Tada, Fusion Eng. Des. **82**, 472 (2007).
[4]R. D. McCarty, *Correlations for the Thermophysical Properties of Deuterium* (National Institute of Standards and Technology, Boulder, CO, 1989).
[5]I. A. Richardson, J. W. Leachman, and E. W. Lemmon, "Fundamental equation of state for deuterium," J. Phys. Chem. Ref. Data (unpublished).
[6]K. Patkowski, W. Cencek, P. Jankowski, K. Szalewicz, J. B. Mehl, G. Garberoglio, and A. H. Harvey, J. Chem. Phys. **129**, 094304 (2008).
[7]A. Michels, W. de Graaff, and C. A. ten Seldam, Physica **26**, 393 (1960).
[8]R. J. Hinde, J. Chem. Phys. **128**, 154308 (2008).
[9]N. Balakrishnan, G. Quéméner, R. C. Forrey, R. J. Hinde, and P. C. Stancil, J. Chem. Phys. **134**, 014301 (2011).
[10]H. Li, A. R. W. McKellar, R. J. Le Roy, and P.-N. Roy, J. Phys. Chem. A **115**, 7327 (2011).
[11]T. H. Dunning, Jr., J. Chem. Phys. **90**, 1007 (1989); R. A. Kendall, T. H. Dunning, Jr., and R. J. Harrison, *ibid.* **96**, 6796 (1992).
[12]F.-M. Tao and Y.-K. Pan, J. Chem. Phys. **97**, 4989 (1992).
[13]K. A. Peterson, D. E. Woon, and T. H. Dunning, J. Chem. Phys. **100**, 7410 (1994).
[14]See supplementary material at http://dx.doi.org/10.1063/1.4757565 for FORTRAN computer code implementing the V_{HP} potential.

[15]S. L. Mielke, B. C. Garrett, and K. A. Peterson, J. Chem. Phys. **116**, 4142 (2002).
[16]W. Kolos, K. Szalewicz, and H. J. Monkhorst, J. Chem. Phys. **84**, 3278 (1986).
[17]M. Galassi, J. Davies, J. Theiler, B. Gough, G. Jungman, M. Booth, and F. Rossi, GNU Scientific Library Reference Manual, Network Theory, Rev. 2nd ed., 2006; see http://www.gnu.org/software/gsl.
[18]G. Garberoglio and J. K. Johnson, ACS Nano **4**, 1703 (2010).
[19]T. Cui, E. Cheng, B. J. Alder, and K. B. Whaley, Phys. Rev. B **55**, 12253 (1997).
[20]M. H. Müser, Mol. Simul. **17**, 131 (1996).
[21]D. Marx and M. H. Müser, J. Phys.: Condens. Matter **11**, R117 (1999).
[22]R. D. Goodwin, D. E. Diller, H. M. Roder, and L. A. Weber, J. Res. Natl. Bur. Stand. **68A**, 121 (1964).
[23]N. Sakoda, K. Shindo, K. Motomura, K. Shinzato, M. Kohno, Y. Takata, and M. Fujii, Int. J. Thermophys. **33**, 381 (2012).
[24]E. W. Lemmon, M. L. Huber, and M. O. McLinden, "REFPROP: Reference fluid thermodynamic and transport properties," NIST Standard Reference Database 23, Version 9.0 (National Institute of Standards and Technology, Gaithersburg, MD, 2010).
[25]G. Garberoglio, M. R. Moldover, and A. H. Harvey, J. Res. Natl. Inst. Stand. Technol. **116**, 729 (2011).
[26]K. Schäfer, Z. Phys. Chem. B **36**, 85 (1937).
[27]J. J. M. Beenakker, F. H. Varekamp, and A. Van Itterbeek, Physica **25**, 9 (1959).
[28]F. H. Varekamp and J. J. M. Beenakker, Physica **25**, 889 (1959).
[29]H. F. P. Knaap, M. Knoester, C. M. Knobler, and J. J. M. Beenakker, Physica **28**, 21 (1962).
[30]M. Jeziorska, P. Jankowski, B. Jeziorski, and K. Szalewicz, J. Chem. Phys. **113**, 2957 (2000).
[31]J. W. Cooley, Math. Comput. **15**, 363 (1961).
[32]J. Rychlewski, Mol. Phys. **41**, 833 (1980).
[33]E. F. May, M. R. Moldover, and J. W. Schmidt, Mol. Phys. **107**, 1577 (2009).
[34]R. J. Hinde, Chem. Phys. Lett. **460**, 141 (2008).
[35]S. Manzhos, K. Nakai, and K. Yamashita, Chem. Phys. Lett. **493**, 229 (2010).